2005

Formation and Growth of Surface Films on Graphitic Anode Materials for Li-Ion Batteries

J. S. Gnanaraj

Robert W. Thompson
Worcester Polytechnic Institute, rwt@wpi.edu

S. N. Iaconatti

J. F. DiCarlo

K. M. Abraham

Electrochemical and Solid-State Letters, **8** (2) A128-A132 (2005)
1099-0062/2005/8(2)/A128/5/$7.00 © The Electrochemical Society, Inc.

Formation and Growth of Surface Films on Graphitic Anode Materials for Li-Ion Batteries

J. S. Gnanaraj,[a,*,z] R. W. Thompson,[a] S. N. Iaconatti,[b] J. F. DiCarlo,[b] and K. M. Abraham[b,*]

[a]*Department of Chemical Engineering, Worcester Polytechnic Institute, Worcester, Massachusetts 01609, USA*
[b]*Yardney Technical Products, Incorporated/Lithion Incorporated, Pawcatuck, Connecticut 06379, USA*

The inductive loop observed in the impedance spectra of the graphite electrode in Li/C cells is attributed to the formation of a $(Li_{1-X}C_6)/C_6$ concentration cell from which current flows in opposition to Li intercalation into graphite, consistent with the conditions for the generation of an inductive loop. The current flow occurs in the $(Li_{1-X}C_6)/C_6$ concentration cell because of the leaky nature of the solid electrolyte interphase (SEI) that isolates Li-rich and Li-deficient islands of carbon or graphite in the electrode during the SEI's formation stage. An equivalent circuit model has been proposed that fits the experimental data well.
 [DOI: 10.1149/1.1850390]

Manuscript submitted August 27, 2004; revised manuscript received October 14, 2004. Available electronically January 6, 2005.

All commercial Li-ion batteries use carbonaceous materials for anodes. Among the various types of carbonaceous materials, natural graphite is the most attractive candidate because of its high theoretical lithium intercalation capacity of 372 mAh/g, abundance, and low cost.[1] However, the flaky graphite particles exfoliate in a number of commonly used electrolyte solutions, especially those based on the high permittivity solvent, propylene carbonate (PC). To solve this problem spherical shaped mesocarbon microbeads (MCMB) are used, but they are relatively expensive and also have lower capacity (320 mAh/g) compared to that of natural graphite. Another option is to modify the surface of the graphite particles either by mild oxidation or by a protective coating of an oxide, metal, polymer, or disordered carbon.[2-4] The disordered carbon coated graphite has been reported to exhibit good electrochemical performance in lithium ion batteries.[4,5] It is generally known that during the first intercalation of lithium into the graphite electrode, the solvent and the lithium salt are reduced to form a surface film called the solid electrolyte interphase (SEI) on graphite electrode. Electrolyte decomposition stops only when the SEI layer is thick enough to prevent electron tunneling through it. The SEI layer thus formed plays a fundamental role in the stability of the graphite electrode assuring it long life and cyclability.[6]

The chemical composition of the SEI formed on carbonaceous anodes is similar to that formed on metallic lithium. However, there are significant differences between metallic lithium and lithiated graphite.[7] As lithium is the most electropositive metal, it reacts spontaneously with the electrolyte to produce various electrolyte reduction components that are more stable thermodynamically than the mother solution, and some of these decomposition products form the SEI film. In contrast, the SEI film on a graphite electrode is formed only when it is polarized from open circuit to lower potentials, and substantial Li intercalation into graphite occurs at potentials below the SEI film formation potential.

The chemical composition of the passivating SEI film has been studied by techniques such as Fourier transform infrared (FTIR) spectrscopy, X-ray photoelectron spectrscopy (XPS), and atomic force micrscopy (AFM) and appears to include the insoluble lithium salts, $(ROCO_2)Li_2$, Li_2CO_3, Li_2O, LiOH, LiF, ROLi, alkoxide, and polymers, where R is typically, CH_2 or C_2H_5 depending on the electrolyte composition.

Electrochemical impedance spectroscopy (EIS) has been used in the past to characterize the surface films on graphite electrodes. To our knowledge, all previous studies involved characterizing the fully developed SEI film, *i.e.*, after the graphite electrode has been fully intercalated with Li, to get information on the film resistance, capacitance, and charge transfer resistance of the electrochemical process. In this work we have used EIS to characterize the potential dependent formation and growth of the SEI film on a pristine natural graphite electrode and a carbon-coated natural graphite electrode in standard electrolyte solutions. These results have provided new insights into the conditions for the formation of a stable SEI on graphites.

Experimental

Pristine natural graphite and carbon coated natural graphite material were provided by Superior Graphite Inc. Chicago, IL, USA. Disordered hard carbon (8.5%) was coated on graphite particles using Fluidized-bed chemical vapor deposition (FCVD) techniques. Scanning electron microscopy (SEM) images showed that the surface of the natural graphite was fully covered uniformly by the disordered carbon. Anodes were prepared by mixing ~1 g of graphite with kynar (PVdF), super P carbon, and NMP solvent. The electrode composition was 87 weight percent (wt %) graphite 10 wt % kynar and 3 wt % super P carbon. The amount of NMP used to make the slurry was adjusted so that the slurry was 47 wt % solids. These materials were coated on copper foil with a metering rod and then vacuum dried at 100°C overnight. The calendared anodes were then punched (1.26 cm^2) and used.

An electrolyte consisting of 1 M $LiPF_6$ in a mixture of ethylene carbonate:diethyl carbonate:dimethyl carbonate (EC:DEC:DMC) (1:1:1,v/v/v) was used. The electrochemical characterization of the electrodes was performed in a three-electrode coin cell (model 2032, NRC Canada).[8] The working electrode was made of graphite and the counter electrode was lithium foil (1.54 cm^2). A Li reference electrode, wrapped around a nickel wire and covered by a piece of separator, was placed between the working electrode and the Li counter electrode foil. These cells were hermetically sealed inside a glove box using standard procedures.

Impedance spectra were measured using the Solartron 1250 frequency response analyzer (FRA) driven by a Pentium pro personal computer. The amplitude of the ac voltage was 5 mV and measurements were carried out in the frequency range of 65 kHz to 5 mHz in automatic sweep mode from high to low frequency with 73 points. All tests were performed at a constant temperature of 20°C in an incubator (VWR, model 2005, USA).

Results and Discussion

A Li/C cell fabricated with freshly prepared natural graphite electrode had an open-circuit potential of *ca.* 3.0 V. The capacity obtained from the natural graphite electrode was 365 mAh/g while that for the carbon-coated graphite was 385 mAh/g.

The Li/C cell was discharged (Li-intercalated) incrementally in potential steps and the impedance was measured at each potential. This allowed us to examine the impedance changes in the early

* Electrochemical Society Active Member.
z E-mail: gnanaraj@wpi.edu

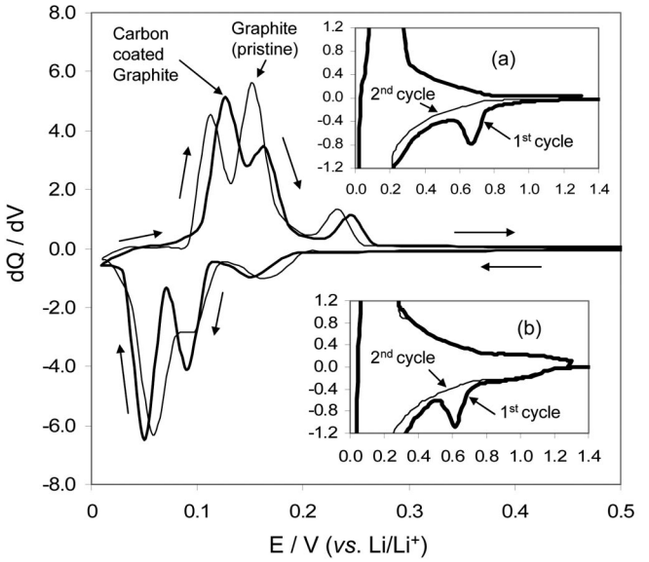

Figure 1. Differential capacity *vs.* voltage obtained from carbon coated natural graphite and noncoated graphite electrodes *vs.* lithium in three electrode coin cell for the first cycle. Insets: expanded view of the differential capacity of first two cycles of (a) noncoated graphite, and (b) carbon coated graphite electrodes. The cells were galvanostatically cycled at the constant current density of 0.2 mA/cm^2. The electrolyte solution used is EC-DMC:DEC (1:1:1)-1 M $LiPF_6$. The electrode area was 1.26 cm^2 and the active mass was ~10 mg.

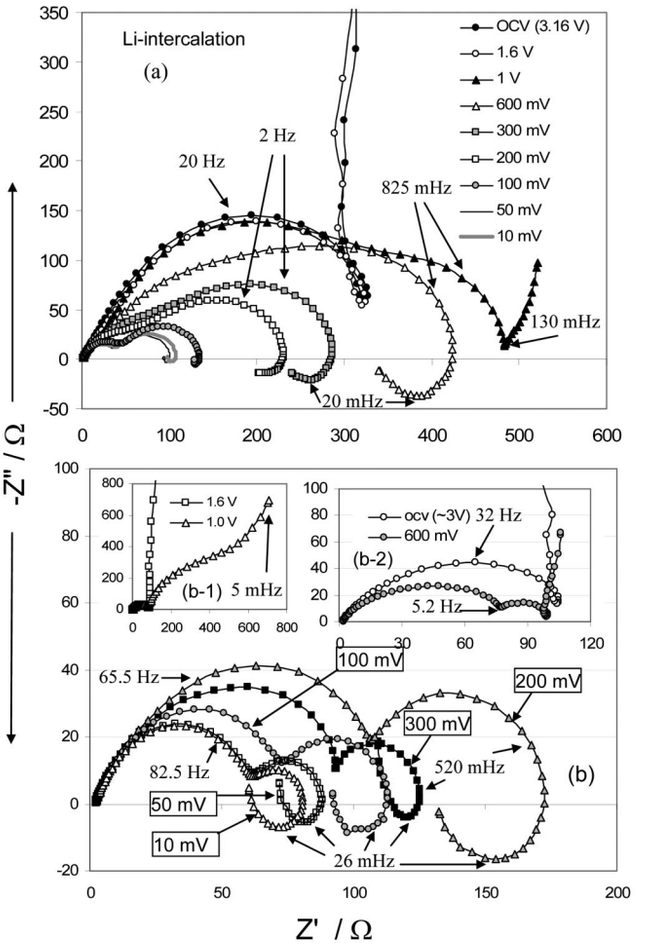

Figure 2. Families of typical Nyquist plots obtained as a function of potential from fresh (a) carbon coated graphite electrode and (b) noncoated graphite electrode *vs.* Li/Li$^+$. The insets show the impedance at (b-1) 1.6 and 1.0 V and, (b-2) OCV, ~3 V and 600 mV. The test was done in a three-electrode coin cell. The electrodes were equilibrated at different potentials (as indicated) from OCV to 10 mV *vs.* Li/Li$^+$ (toward Li-intercalation direction) during the first cycle for several hours before the EIS measurements. The electrolyte used was EC:DEC:DMC (1:1:1) 1 M $LiPF_6$. Active electrode mass ~10 mg. Frequency range 65 kHz-5 mHz. A few frequencies are indicated.

stages of the SEI formation and to determine the manner in which the Li intercalation influences the impedance spectra. Specifically, the cell was discharged galvanostatically to a potential step at a current density of 0.2 mA/cm^2 and was then held at that potential for several hours until the current decayed to a few microamperes. Impedance was measured at each potential step at open circuit. The same procedure was followed during both Li-intercalation and deintercalation cycles.

Figure 1 shows the differential capacity (dQ/dV) *vs.* voltage for the noncoated (pristine) and carbon-coated natural graphite electrodes obtained from the first discharge/charge cycle. Both electrodes show three reversible cathodic peaks below 0.3 V (*vs.* Li/Li$^+$) during Li intercalation and deintercalation cycles. It is well established that these three cathodic peaks correspond to the Li staging in the graphite electrode: the diluted stage I to stage IV, stage III to stage II, and stage II to stage I transitions respectively.[9-11] During Li deintercalation reaction, three peaks due to the reverse processes corresponding to the three stages appear in the anodic direction. The insets in Fig. 1 present the expanded y-axis of the differential capacity for the first two cycles. Both electrodes show an irreversible peak at around 0.6 V (*vs.* Li/Li$^+$) for a cathodic process that begins at ~1 V. It is pronounced only during the first cathodic wave and is ascribed to the reduction of the solution to form insoluble surface species, or the SEI film, that passivate the electrodes (*e.g.*, $ROCO_2Li$ formed by solvent reduction, LiF formed by $LiPF_6$ reduction, and LiOH formed by trace water reduction).[12-15] A pronounced reversible step starting from 1.2 V (*vs.* Li/Li$^+$) is observed in the carbon-coated graphite electrode which is not seen in the noncoated graphite electrode. It is believed that this peak corresponds to insertion of Li into disorder carbon.[16-18]

Figure 2a shows families of impedance spectra obtained during the first Li-intercalation half cycle from a freshly prepared carbon-coated graphite electrode as a function of potential. The impedance spectra obtained at open-circuit voltage (OCV), (3.16 V) and at 1.6 V show a single high-frequency (HF) arc and a straight line perpendicular to the x-axis (Z') in the low-frequency region that represents the blocking character of nonlithiated electrode at equilibrium potential. The size of the HF arc is not changed over the potentials from OCV (~3) to 1 V. The impedance measured at 1 V shows two overlapping semicircles at high- to medium-frequency regions and a straight slanting line at the low-frequency region. Starting with 600 mV the impedance spectra show two semicircles at the low-frequency region, one above the real axis and one below the real axis. The latter has the characteristics of an inductive loop. The size of these low-frequency semicircles above and below the real axis decreases as the polarization potential decreases.

Figure 2b shows families of impedance spectra of the noncoated (pristine) graphite electrode. The impedance spectra obtained at OCV (3.16 V) and at 1.6 V also show a single high-frequency arc and a straight line perpendicular to the x-axis (Z') in the low-frequency region. The spectrum measured at 1 V shows two overlapping semicircles at high- to medium-frequency regions and a straight line at the low-frequency region. However, the size of the high-frequency arc changes as the potential changes from OCV (~3 V) to 1 V.

The impedance spectrum measured at 600 mV for the noncoated (pristine) graphite electrode shows two loops of different diameters

above the real axis at high- to medium-frequency region. Interestingly, an inductive loop appears below the real axis at 300 mV and the size of this inductive loop increases until the potential is 200 mV and then decreases as the polarization potential decreases. These changes may be associated with the changes in the resistance of the electrode accompanying Li intercalation and SEI growth at these potentials.

The high-frequency arc before the SEI formation may be attributed to the impedance from grain boundaries in the composite anode. This is consistent with the observations of Holzapfel *et al.*[17] who proposed that the appearance of HF arc before the surface film formation should be attributed to contact problems between different phases or different particles and to the reduction of absorbed gas (*e.g.*, oxygen) in the electrode, factors related to a composite electrode. Other researchers related the HF arc to the non-ideal behavior of the composite electrode, *e.g.*, porosity of the material, roughness, of the surface.[15,18,19] Note that the size of the high-frequency arc is not changed much when the potential is decreased from OCV (~3 V) to 1 V in the carbon-coated graphite electrode. This may be due to the uniform coating of the hard disordered carbon. Whereas in the case of noncoated graphite (pristine) electrode, the decreasing high-frequency arc size may reflect the changing electronic conductivity of the graphite electrode as the potential is swept from OCV to lower values.

The differential capacity indicates that the Li intercalation into carbon occurs at ~1 V (a hump in Fig. 1b) and no Li intercalation is expected in pristine graphite electrode at that potential (Fig. 1a). However, the impedance measured at 1 V for both electrodes show that the high-frequency arc overlaps with a medium-frequency arc related to charge transfer resistance and that is followed by a low-frequency Warburg impedance spike. The charge transfer resistance (medium-frequency arc) at 1 V may be due to the reduction of water molecules.[16,20] Because water is present only in trace quantities as an impurity, its reduction peak would not be seen in the differential capacity plot either. It is also possible that this medium-frequency arc is due to Li insertion into the high surface area super P carbon that is used to enhance electronic conductivity in the electrode. A reduction peak for Super P carbon is not seen in the differential capacity plot because Li intercalation into Super P occurs in a potential range between ~1 and 0.0 V for which no peak would be seen in the differential capacity plot.

An important feature of the impedance spectra is the appearance of the inductive loop beginning ~1 V. An inductance is defined as the property of an electric circuit that causes an electromotive force to be generated in it as a result of a change in the current flowing through the circuit. The inductive loop first appears at the potential region where Li intercalation into either super P carbon or disordered carbon begins, and then continues into the potential region where Li is intercalated into graphite. A plausible explanation for the inductive loop is the formation of an electromotive force superimposed on the Li intercalation. Most likely it results from concentration cell established between graphite (C_6) and lithiated carbon or lithiated graphite ($Li_{1-X}C_6$) separated by the growing surface film (SEI). Because the surface film is imperfect during the growth stage a current flows between the electrodes in the concentration cell, generating a field that opposes the field due to the intercalation reaction. The discharge of a concentration cell involves current flow opposed to charging the carbon anode with Li. Such a situation meets the requirements for the formation of an inductive loop. To understand an inductive loop in the cell, a pictorial representation of surface film growth on graphite electrode is presented in Fig. 3. In a Li/C cell, during the first cathodic cycle the surface film initially forms beginning at about 1 V as islands on the surface of the graphite electrode. When Li is intercalated into carbon or graphite there is some isolation of Li-rich and Li-poor (deficient) regions in the electrode by the surface film leading to a current flow that opposes the primary intercalation reaction. The $(Li_{1-X}C_6)/C_6$ concentration cell continues to leak current until the electrode is fully intercalated, *i.e.*, the Li concentration differences in the electrode are removed. The initial surface film may be termed a 'leaky surface film'. Once a stable surface film is formed after several charge/discharge cycles the inductive loop disappears as the electrode has acquired a stable nonleaky surface film and has established equilibrium with respect to electronic continuity. Note that several recent studies have found low-frequency inductive loops in the first Li-intercalation in Li/C cells.[18,19,21] However, no satisfactory explanation for this phenomenon has been given until this work. The previous explanation of adsorption is unsatisfactory because adsorption does not involve charge transfer which is required for observing an inductive effect.

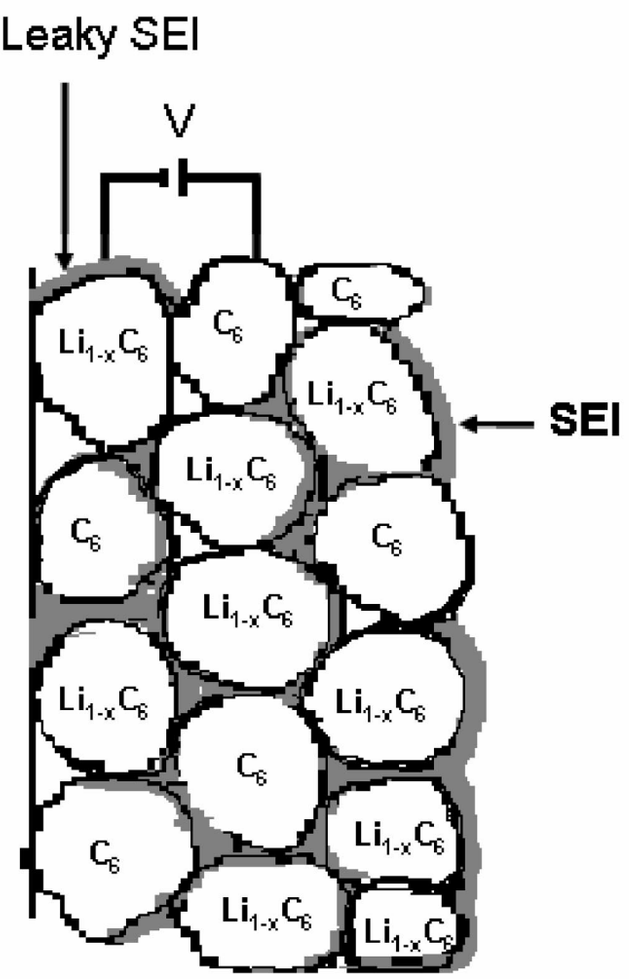

Figure 3. Pictorial representation model for the SEI film growth and the concentration cell.

We used an equivalent circuit shown in Fig. 4a to analyze the measured impedance data. The circuit model involves three regions connected in series: a series resistance; a constant phase element (CPE) parallel with a resistance; another parallel capacitance and resistance, followed by a series circuit of parallel resistance and inductance elements. The CPE is a capacitive element usually related to the electrode roughness,[22] inhomogeneous reaction rates on a surface (*e.g.*, polycrystalline metal surfaces or carbon electrodes with a distribution of active sites),[23] and varying thickness or composition of a coating.[24]

The impedance of an equivalent circuit for a parallel combination of CPE and R could be expressed by

$$Z(\omega) = \frac{R}{1 + (j\omega)^{\alpha}CR} \qquad [1]$$

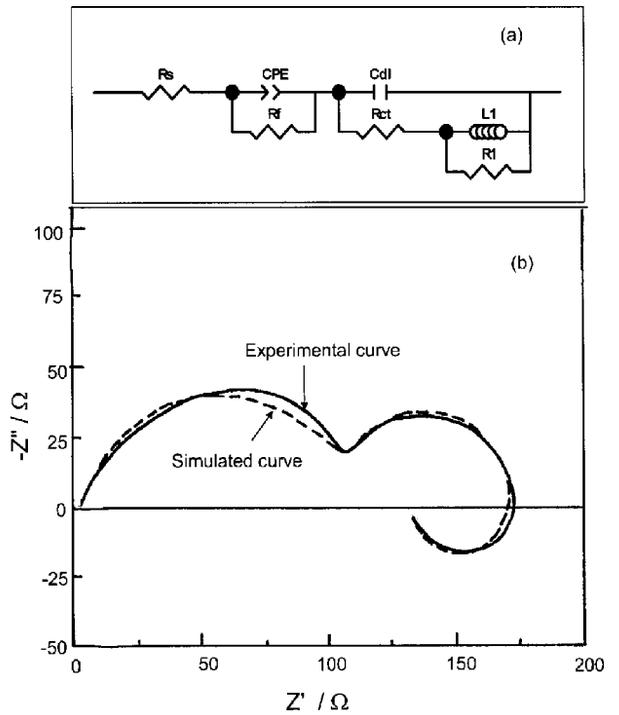

Figure 4. (a) Equivalent circuit model used to fit (b) an experimental impedance curve measured from graphite electrode at 200 mV *vs.* Li/Li^+.

where α is equal to 1 for a pure capacitance, and less than 1 for CPE.

Figure 4b presents a typical impedance plot measured at 200 mV from graphite pristine electrode and the simulated curve using the model (Fig. 4a). A Z-plot was used to fit the experimental curve using values presented in Table I. As can be seen the simulated curve fits the experimental data very well. However, detailed interpretation of the individual components is beyond the scope of this work and is not discussed here.

Recently, Vorotyntsev *et al.*[25] reported a time difference impedance for the growing part of the surface film on lithium metal in EC:DDMC:1 M $LiAsF_6$ solution and proposed that the subtraction of the time difference impedance plot measured at the time intervals closest to the electrode's preparation of the film formation showed two loops of different diameters above and below the real axis while the subsequent time difference plots showed a quite different behavior of regular loop, a depressed semicircle without any points in the lower half of the complex plane (below the real axis). The loop below the real axis of the impedance was explained in terms of the rapid evolution of local characteristics of the film growth, although the nature of those local characteristics were not discussed.[25] Note that Li intercalation into carbon/graphite is crucial to the onset of the impedance loop in the impedance spectra measured in this work.

Table I. Values of the equivalent circuit components used for fitting the experimental curve.

Components	Description	Fitted values
Rs	Solution resistance	2.937 Ω
Rf	Resistance of the surface film (SEI) layer	107.000 Ω
CPE	Constant phase element of the SEI layer	55.011 μF
α	Power factor	0.800
R(CT)	Resistance of the charge transfer reaction	23.980 Ω
C(CT)	Double layer capacitance	2.434 mF
L	Inductance	70.000 H
R(leaky SEI)	Resistance of the leaky SEI layer	36.690 Ω

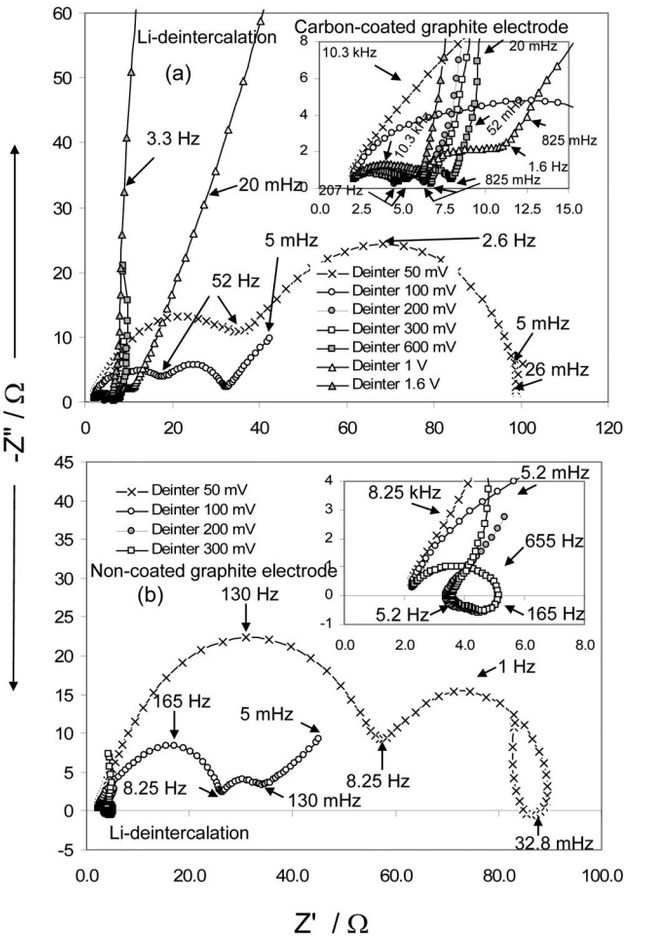

Figure 5. Same as Fig. 2, in the anodic direction. The insets in (a) and (b) relate to high frequency domain.

The impedance spectra measured on the anodic direction (going from 10 mV to 1.6 V *vs.* Li/Li^+) at different potentials are presented in Fig. 5 for (a) carbon coated graphite and (b) noncoated graphite electrode. The size of the impedance spectra arc in the high-medium frequency region observed at 50 mV on the anodic direction is comparable to that observed at 50 mV on the cathodic direction. Note that the impedance spectra measured in the potential region 100-300 mV in the anodic direction have loops below the real axis (Fig. 5b). This further supports our model for the origin of the inductance arc since Li-rich and Li-poor regions are created in the electrodes while Li is removed from the electrode. The size of the impedance arc at high-medium frequency decreases drastically as the deintercalation starts above 100 mV and continues to decrease until it reaches the deintercalation potential 200 mV. The size of the impedance arc increases as the potentials goes further to positive directions to 600 mV.

Figure 6 shows impedance spectra measured after the cell is fully stabilized by cycling galvanostatically five times at the current density of 0.2 mA/cm^2. The high-frequency arc related to the grain boundaries in the composite anode will be dominated by the surface film once the cell is stabilized. It is evident from the figure that the size of the high-frequency arc related to surface film is invariant with potential while the medium-frequency arc related to charge transfer varies with potential as expected. This indicates that the SEI formed is robust. In parallel to disappearance of inductive loop in

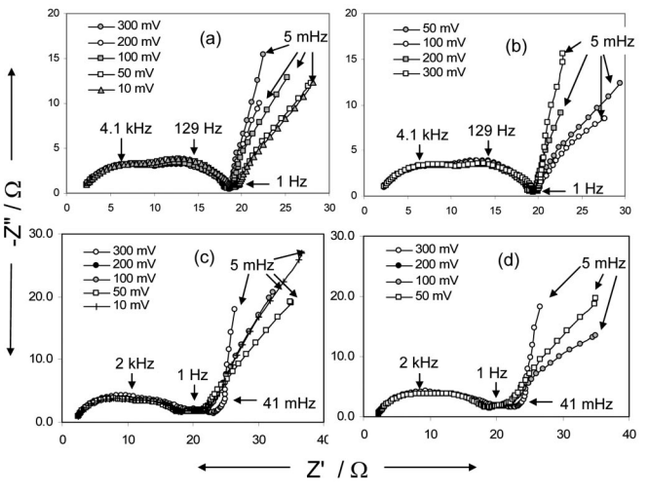

Figure 6. Impedance spectra obtained at different potentials from fresh (a and b) carbon coated graphite electrode and (c and d) noncoated graphite electrode *vs.* Li/Li^+ after few galavnostaic cycling at 0.2 mA/cm^2 during (a and c) Li-intercalation and (b and d) Li-deintercalation direction (as indicated). Few frequencies are also indicated in the figure.

the medium-frequency impedance spectra of well-cycled electrode (Fig. 6) one can see a typical development of low-frequency arcs or a tendency to form low-frequency semicircle as is predicted by recent models.[26,27] Our result suggest that the impedance spectra can be used as a tool to check the SEI film formation, growth, and its robustness on carbon or graphite anodes in Li-ion batteries.

Conclusions

Natural graphite and carbon-coated natural graphite electrodes have been studied by measuring impedance spectra as a function of potentials. The impedance spectra showed inductive loops beginning at and continuing into potentials where Li intercalation occurs in carbon or natural graphite. We attribute the inductive loop to the formation of a $(Li_{1-X}C_6)/C_6$ concentration cell from which current flows in opposition to Li intercalation into graphite, consistent with the conditions for the generation of an inductive loop. The current flow occurs in the $(Li_{1-X}C_6)/C_6$ concentration cell because of the leaky nature of the SEI that isolates Li-rich and Li-deficient islands of carbon or graphite in the electrode during the SEI's formation stage. Once a stable SEI has been formed the inductive loop does not appear in the impedance spectra. An equivalent circuit model has been proposed that fits the experimental data well. The formation and disappearance of the inductive loop in the impedance spectra of carbon anodes in the 'formation cycles' of Li-ion batteries may be used to assess the robustness of the SEI on the anode. An impedance spectrum without an inductive loop at potentials where substantial Li intercalation occurs may be indicative of a robust SEI on the carbon anode.

Acknowledgment

The authors thank the U.S. Army Space and Missile Defense Command (SMDC) under contract no. DASG60-03-C-0073 and the U.S. Air Force under contract no. F-33615-98-2898 for financial support of this work.

Worcester Polytechnic Institute assisted in meeting the publication costs of this article.

References

1. J. M. Tarascon and M. Armand, *Nature (London)*, **414**, 359 (2001).
2. Y. P. Wu, E. Rahm, and R. Holze, *J. Power Sources*, **114**, 228 (2003).
3. S. S. Zhang, K. Xu, and T. R. Jow, *Electrochem. Commun.*, **5**, 979 (2003).
4. M. Yoshio, H. Wang, and K. Fukuda, *Angew. Chem., Int. Ed. Engl.*, **42**, 4203 (2003).
5. I. Kuribayashi, M. Yokoyama, and M. Yamashita, *J. Power Sources*, **54**, 1 (1995).
6. E. Peled, *J. Electrochem. Soc.*, **145**, 172 (1998).
7. M. Winter and J.-O. Besenhard, in *Handbook of Battery Materials*, J.-O. Besenhard, Editor, Wiley, New York (1999).
8. J. S. Gnanaraj, M. D. Levi, Y. Gofer, M. Schmidt, and D. Aurbach, *J. Electrochem. Soc.*, **150**, A445 (2003).
9. J. R. Dahn, *Phys. Rev. B*, **44**, 9170 (1991).
10. T. Ohzuku, Y. Iwakoshi, and K. Sawai, *J. Electrochem. Soc.*, **140**, 2490 (1993).
11. Z. Jiang, M. Alamgir, and K. M. Abraham, *J. Electrochem. Soc.*, **142**, 333 (1995).
12. D. Aurbach, Y. Ein-Eli, B. Markovsky, A. Zaban, S. Luski, Y. Carmeli, and H. Yamin, *J. Electrochem. Soc.*, **142**, 2882 (1995).
13. K. Kanamura, H. Tamura, S. Shiraishi, and Z.-I. Takehedra, *J. Electroanal. Chem.*, **394**, 49 (1995).
14. E. Peled, D. Golodnitsky, and G. Ardel, *J. Electrochem. Soc.*, **144**, L208 (1997).
15. S. S. Zhang, M. S. Ding, K. Xu, J. Allen, and T. R. Jow, *Electrochem. Solid-State Lett.*, **4**, A206 (2001).
16. J. S. Gnanaraj, M. D. Levi, E. Levi, G. Salitra, D. Aurbach, J. E. Fischer, and A. Clay, *J. Electrochem. Soc.*, **148**, A525 (2001).
17. M. Holzapfel, A. Martinent, F. Alloin, B. Le Gorrect, R. Yazami, and C. Montella, *J. Electroanal. Chem.*, **546**, 41 (2003).
18. R. Takasu, K. Sekine, and T. Takamura, *J. Power Sources*, **81-82**, 224 (1999).
19. J. Y. Song, H. H. Lee, Y. Y. Wang, and C. C. Wan, *J. Power Sources*, **111**, 255 (2002).
20. D. Aurbach, M. L. Daroux, P. Faguy, and E. B. Yeager, *J. Electroanal. Chem. Interfacial Electrochem.*, **297**, 225 (1991).
21. M. Itagaki, N. Kobari, S. Yotsuta, K. Watanabe, S. Kinoshita, and M. Ue, *J. Power Sources*, **135**, 255 (2004).
22. W. H. Mulder, J. H. Sluytes, T. Pajkossy, and I. Nyikos, *J. Electroanal. Chem.*, **285**, 103 (1990).
23. C.-H. Kim, S.-I. Pyun, and J.-H. Kim, *Electrochim. Acta*, **48**, 3455 (2003).
24. C. A. Schiller and W. Strunz, *Electrochim. Acta*, **46**, 3619 (2001).
25. M. A. Vorotyntsev, M. D. Levi, A. Schechter, and D. Aurbach, *J. Phys. Chem. B*, **105**, 188 (2001).
26. J. P. Meyers, M. Doyle, R. M. Darling, and J. Newman, *J. Electrochem. Soc.*, **147**, 2930 (2000).
27. M. D. Levi and D. Aurbach, *J. Phys. Chem. B*, **108**, 11693 (2004).